Scientia Iranica (2024) 31(19), 1825–1841

Sharif University of Technology
Scientia Iranica
Transactions A: Civil Engineering
https://scientiairanica.sharif.edu

Strength prediction of composite metal deck slabs under free drop weight impact loading using numerical approach and data set machine learning

Fakhreddin Emami, and Mohammad Zaman Kabir*

Department of Civil and Environmental Engineering, AmirKabir University of Technology, Tehran, Iran.

Received 17 December 2021; received in revised form 7 May 2022; accepted 5 April 2023

KEYWORDS
Composite metal deck slab;
Finite element analysis;
Machine learning;
Impact loading;
Negative moment.

Abstract. Structural systems may experience negative moments due to dynamic excitations and inertia effects. Composite metal deck slabs are typically designed to withstand positive moments and reinforced at the bottom, with minimal thermal reinforcement at the top. However, under dynamic impact loading, insufficient reinforcement at the upper part may cause these slabs to fail under negative moments. Therefore, this study investigates the performance of composite metal deck slabs under free drop weight impact loading. The research consists of two main parts: generating a data set through finite element simulation analysis and training machines based on the collected data. The LS-DYNA commercial software was used to analyze 165 models with three parameters: slab lengths, striker weights, and striker velocities. In the machine learning component, the Finite element modeling (FEM) results were utilized to train the machines and to accurately predict the performance of these slabs. The outcomes were reported in terms of the maximum negative moment, maximum deflection, and elastic and plastic behaviour of the slab. The study revealed that at high striker velocities, the specimens experienced an ultimate internal negative moment within the range of 60 to 80 kN.m.

1. Introduction

1.1. Overview

When it comes to constructing building floors, composite metal deck slabs are often the preferred option. This type of structural system usually includes a metal deck sheet, concrete slab, shear studs, thermal reinforcement, and girders. The metal deck sheet serves two main functions within this system: providing a framework for construction and reinforcement for the tensile concrete component [1]. Figure 1 [2] depicts the schematic arrangement of this system. The use of composite metal deck slab system as a dependable flooring system in the industry offers numerous benefits. These include fast construction, no need for jacking support,

*. *Corresponding author.*
E-mail address: mzkabir@aut.ac.ir (M.Z. Kabir)

To cite this article:
F. Emami and M.Z. Kabir "Strength prediction of composite metal deck slabs under free drop weight impact loading using numerical approach and data set machine learning", *Scientia Iranica* (2024), **31**(19), pp. 1825–1841
https://doi.org/10.24200/sci.2023.59582.6321

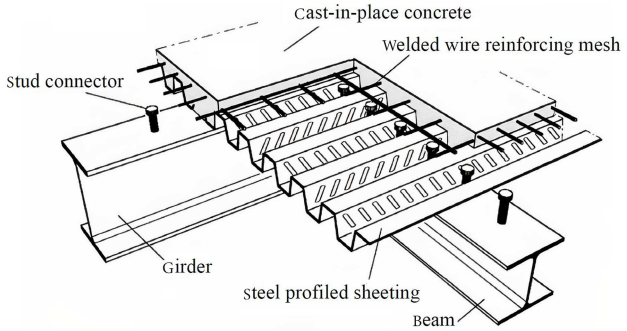

Figure 1. Composite floor with steel profile sheeting [2].

a lightweight structural system, ease of handling and installation, and high strength. However, there are also some limitations to this system. Despite the metal deck serving as the bottom reinforcement in the design, there is minimal thermal reinforcement provided for the top part of the structural system. The performance of the composite slab system is generally satisfactory as long as it is not exposed to significant negative moment. However, sudden and substantial negative moment can lead to potential failure and compromise the composite performance and structural integrity of the system, particularly near the supports. This scenario is more likely to occur when the flooring is expected to bear high dynamic impact loading, which may generate negative moments in the structural flooring system even in the case of simply supported slabs.

While there are dependable methods available for analyzing structural components that undergo static loads [3–7], designing and analyzing structural systems under extreme dynamic excitation, such as impact loading, can be challenging for design engineers. One alternative solution for designers is to employ incremental dynamic analysis, which involves assessing both load and material properties in the static domain [8]. However, conducting finite element analysis and experimental testing are more precise approaches, as noted by numerous researchers [9–18]. Several researchers have studied the behavior of reinforced concrete slabs and beams under dynamic loading [8,19–23]. However, only a handful of studies have focused on composite metal deck slabs [24,25], with researchers employing numerical and experimental approaches to address the associated issues. The limited research and the weakness of composite metal deck slabs in resisting negative moments create a knowledge gap, leading to a partial understanding of the design and performance of this flooring system under severe dynamic loads. This study aims to bridge this gap by expanding knowledge and providing more information on this topic.

1.2. Research goal

In modern times, researchers often turn to machine-learning techniques to improve the computational aspects of engineering applications [26–41]. The focus

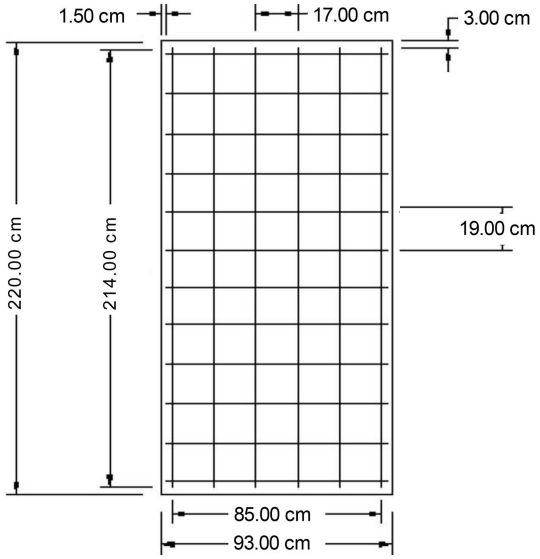

Figure 2. Details of reinforcing in specimens.

of this paper is to develop a computational approach that accurately models the behavior of composite metal decks when subjected to free drop weight impact loading. The initial steps involved conducting a parametric study using finite element simulation and analysis. Subsequently, a finite dataset was generated to facilitate the use of Machine Learning (ML) algorithms for training machines in the next stage of the computational approach. Trained machines are capable of predicting the performance of thousands of models within a very short period of time. Therefore, the second phase of the computational approach can be regarded as a time-efficient alternative to the first phase, with less computational cost. However, the accuracy of the predictions relies on several factors, such as the level of correctness of the trained machines, the size of the dataset used for training the machines, and the arrangement and correlation of data within the dataset.

The proposed computational approach is anticipated to enhance the understanding of the performance of composite metal deck slabs under impact loading. Three key domains are slated for examination:

- The elastic and plastic behavior of slabs;
- The maximum deflection;
- The maximum negative moment.

1.3. Numerical model

The initial accepted model for this section is a drop weight impact test on a composite metal deck slab, as described in reference [20]. The slab model measures 2200 mm in length and 930 mm in width, with a variable thickness ranging from 50 to 115 mm. The thermal metal bars and cross-section of the metal deck sheet are shown in Figures 2 and 3, respectively. The thermal metal bars have a diameter of 6.5 mm, while

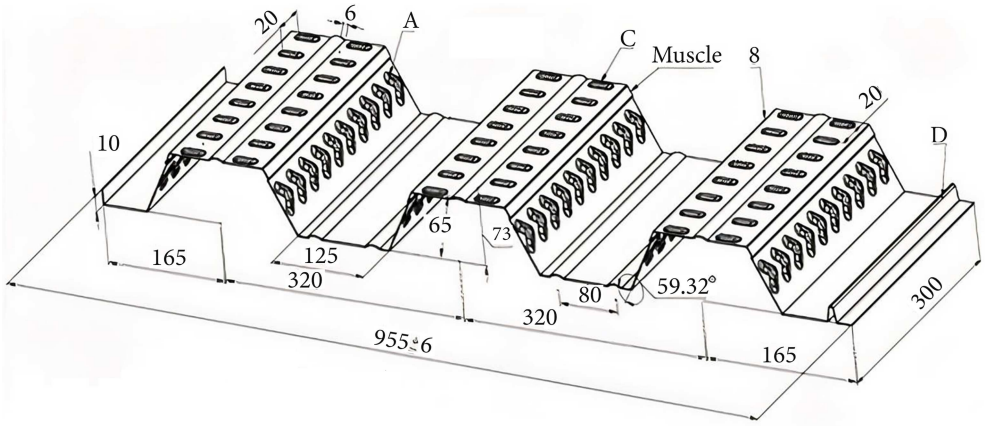

Figure 3. The shape and properties of the metal deck and dimensions are in mm.

the metal deck sheet has a thickness of 1 mm. A girder in the form of an IPE300 flange is used as a fixture. The shear stud measures 90 mm in overall length, with an 80 mm body and a 10 mm head. The head diameter is 35 mm, and the body diameter is 22 mm.

The LS-DYNA environment was utilized for constructing numerical FE models of the components mentioned. To account for the dynamic excitation nature of loading, the dynamic explicit option was also chosen as the analyzing method. Numerical simulations included three types of elements: solid, shell, and truss. The concrete slab, shear studs, rigid fixture, and striker were modeled using eight-node solid elements, each with three translation degrees of freedom per node. The metal deck sheet was modeled using quadrilateral shell elements with four nodes per element, with membrane and bending behavior. Each node of these shell elements had three translational and rotational degrees of freedom. For the remaining components, which were thermal bars, 3D 2-node truss elements with three translational degrees of freedom per node were used. The mesh size for the numerical model elements was optimized through a convergence study, resulting in the mesh size used in this work [25].

The selection of an appropriate material is crucial when numerically modeling structures subjected to impact loading, especially for nonlinear analysis. At high strain rates, materials can exhibit unexpected behavior. Concrete and steel, for example, are more prone to brittle response and higher strength under such conditions. To model the concrete part in the present study, MAT-CMCS (Material 159) was chosen due to concrete's strain rate dependence. The continuous surface cap model (CSCM), which is widely used by researchers to capture concrete behavior under high strain rate loading, was employed. Table 1 [25] provides details of the material properties used in the numerical simulation for concrete.

The current CSCM model is defined by 37 input parameters. These parameters were determined using

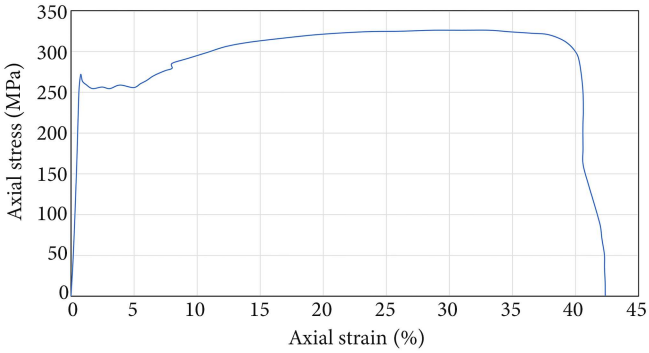

Figure 4. Engineering stress-strain diagram for the metal deck.

Table 1. Material properties of concrete [25].

Density (kg/m^3)	2400
Compressive strength (MPa)	30
Tensile strength (MPa)	2.8
Elastic modulus (GPa)	30
Shear modulus (GPa)	18
Poisson's ratio	0.18

the User's Manual for LS-DYNA Concrete Material Model 159 [47], based on the unconfined compression strength and aggregate size. For concrete aggregates, ASTM C136 [48] was used for sieve analysis, with no size greater than 19 mm. The material model for the metal deck and shear studs is MAT-PIECEWISE-LINEAR-PLASTICITY (Materials 24), which accounts for strain rate effects and nonlinear properties. Deck stress-strain data points were derived from the diagram in Figure 4, which was obtained using an engineering stress-strain diagram based on ASTM A370 [49] and a metal deck coupon. These data points were then converted to true values in the material model. The material model for steel bars is MAT-

Table 2. Material properties of metal deck [20].

Density (kg/m^3)	7850
Yield stress (MPa)	275.8
Ultimate stress (MPa)	336.77
Elastic modulus (GPa)	170
ε_{ult} (%)	30.76
Poisson's ratio	0.3

Table 3. Material properties of metal bars [25].

Density (kg/m^3)	7850
Yield stress (MPa)	331.22
Ultimate stress (MPa)	456.51
Elastic modulus (GPa)	200
ε_{ult} (%)	18.55
Poisson's ratio	0.3

Table 4. Material properties of metal shear studs [25].

Density (kg/m^3)	7850
Yield stress (MPa)	347.43
Ultimate stress (MPa)	559.62
Elastic modulus (GPa)	200
ε_{ult} (%)	28.31
Poisson's ratio	0.3

PLASTIC-KINEMATIC (Materials 3). Tables 2, 3, and 4 show the material properties for metal deck sheet, steel bars, and shear studs, respectively [25]. Since the fixture and striker are assumed to be rigid bodies, a rigid material with a density of 7850 kg/m^3 was chosen for them. As previously mentioned, defining the strain rate is an important aspect of numerical modeling due to the high velocity of impact loading. To account for the effect of strain rate on steel materials, the CEB code criteria were applied [50]. The following equations, namely the Dynamic Increase Factor (DIF) formulas (Eqs. (1) and (2)), were used for the steel material to incorporate strain rate effects:

$$DIF_{(steel\ yield)} = \left(\frac{\dot{\varepsilon}}{10^{-4}}\right)^{0.074+0.4\frac{f_y}{414}}, \quad (1)$$

$$DIF_{(steel\ yield)} = \left(\frac{\dot{\varepsilon}}{10^{-4}}\right)^{0.019+0.01\frac{f_u}{414}}. \quad (2)$$

In which $\dot{\varepsilon}$, f_y, and f_u are steel strain rate, steel yield stress and steel ultimate stress, respectively. To model interfaces between components of the model, the contacts are introduced as AUTOMATIC-SURFACE-to-SURFACE and AUTOMATIC-SURFACE-to-SURFACE-TIEBREAK. A friction coefficient of 0.13 is assumed between the deck and the slab. Table 5 provides information on the contact types between various parts of the model.

To reduce computational running time, only one-quarter of the composite slab was modeled, as shown in Figure 5. The x-y and y-z planes are planes of symmetry for both the slab geometry and applied load in this model. The impact load was applied by the rigid striker and allowed to move only in the y direction, with a specified initial velocity [25]. Figure 6 depicts the boundary conditions applied to the parts in the model. In this figure, X, Y, and Z represent the translational degree of freedom, while RX, RY, and RZ indicate rotational angles with respect to the X, Y, and Z axes, respectively.

1.4. Proposed parametric studies

A verified model is used to conduct a parametric study, with the slab length, striker weight, and striker velocity being the three primary variables. Table 6 summarizes the suggested parameter ranges. FEM analysis results are presented in Figure 7, which display the relationship between the parameters (slab length, striker

Table 5. Contact types between different parts [25].

Striker-Slab	AUTOMATIC-SURFACE-to-SURFACE
Striker-Deck	AUTOMATIC-SURFACE-to-SURFACE
Striker-Bars	AUTOMATIC-SURFACE-to-SURFACE
Fixture-Slab	AUTOMATIC-SURFACE-to-SURFACE
Fixture-Deck	AUTOMATIC-SURFACE-to-SURFACE
Fixture-Bars	AUTOMATIC-SURFACE-to-SURFACE
Shear studs-Slab	AUTOMATIC-SURFACE-to-SURFACE
Shear studs-Deck	AUTOMATIC-SURFACE-to-SURFACE
Shear studs-Bars	AUTOMATIC-SURFACE-to-SURFACE
Shear studs-Slab	Tied
Deck-Fixture (for elements around shear studs)	Tied
Deck-Slab	AUTOMATIC-SURFACE-to-SURFACE-TIEBREAK

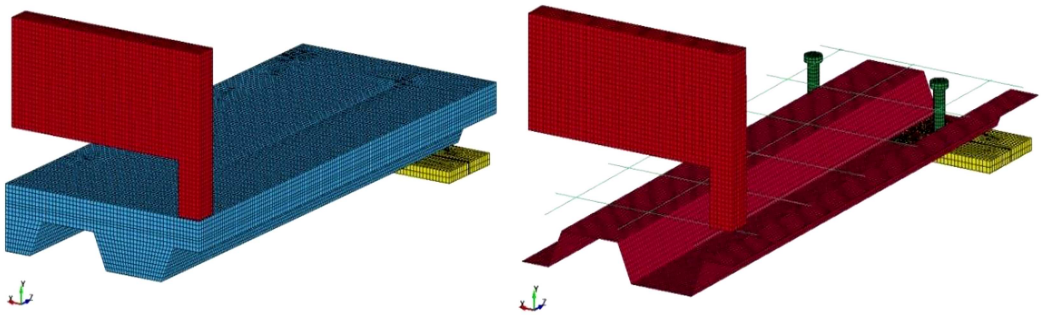

Figure 5. One quarter FE model in LS-DYNA.

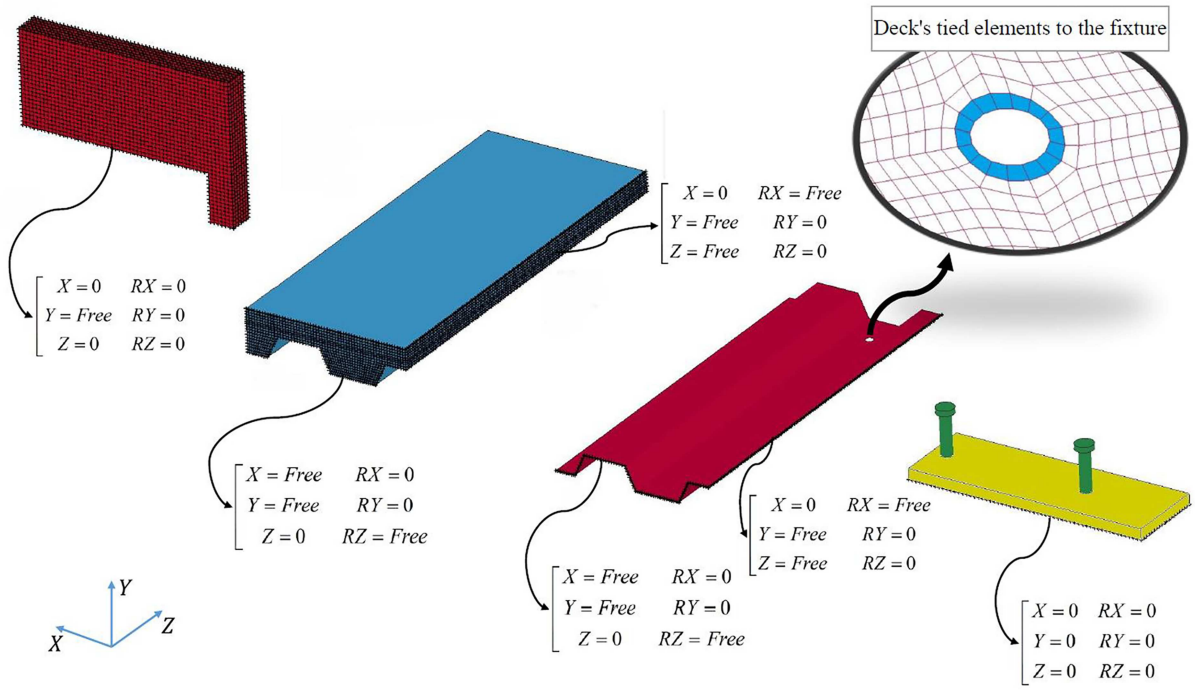

Figure 6. Details on boundary conditions in the model.

velocity, and striker weight) and the corresponding outcomes (maximum negative moment or maximum deflection). Based on the plots in Figure 7, the following trends can be observed:

- The maximum negative moment should not exceed 70 kN.m for striker velocities greater than 3600 mm/s and striker weights greater than 400 kg;
- The maximum negative moments remain constant when they reach the ultimate limit, while the deflection continues to increase;
- The plastic deflection range is significantly larger than the elastic deflection range;
- The plastic distribution shifts to the right side in striker velocity distribution plots and has less overlap with the elastic distribution. This separation is more pronounced when the distribution is based on striker weights;

Table 6. Outline of parametric studies.

Slab length (m)	Striker weight (kg)	Striker velocity (mm/s)
2	25/ 50/ 75/ 100/ 150/ 200/ 300/ 400/ 600/ 800/ 1000	1600/ 2600/ 3600/4600/ 5600
2.5	25/ 50/ 75/ 100/ 150/ 200/ 300/ 400/ 600/ 800/ 1000	1600/ 2600/ 3600/ 4600/ 5600
3	25/ 50/ 75/ 100/ 150/ 200/ 300/ 400/ 600/ 800/ 1000	1600/ 2600/ 3600/4600/ 5600

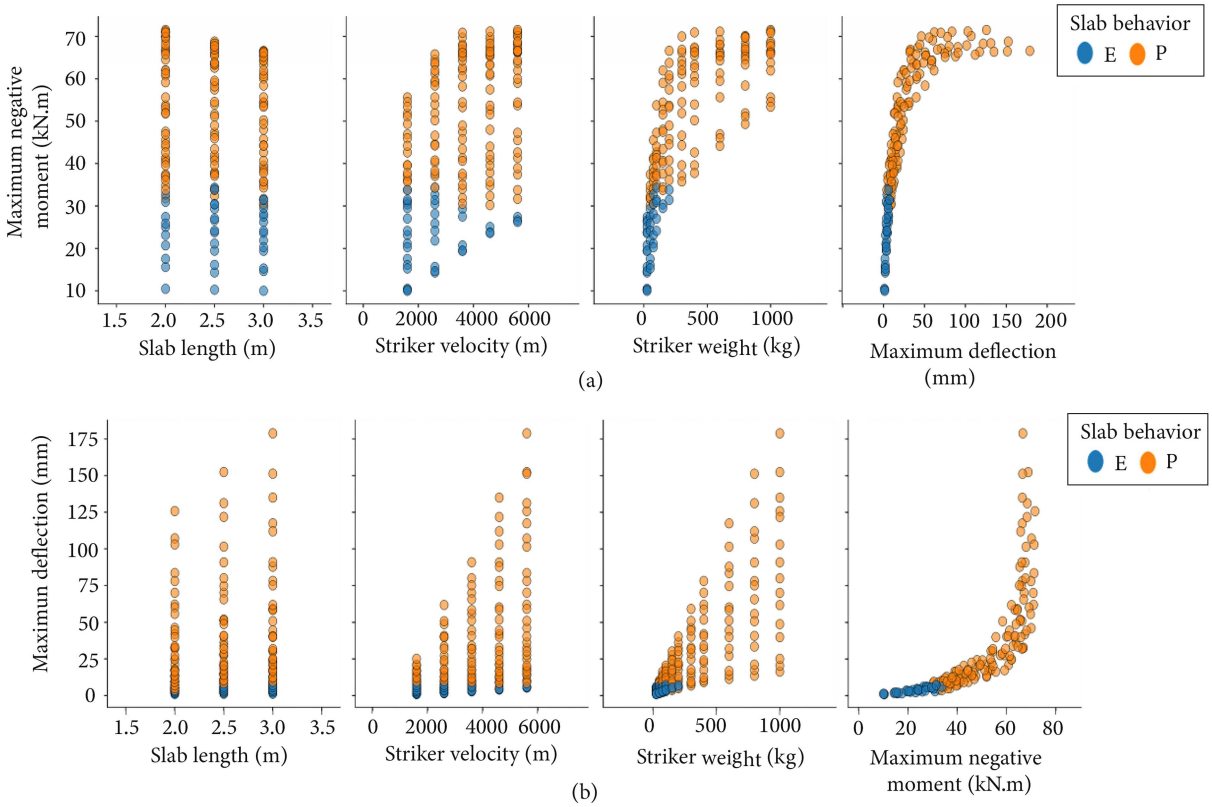

Figure 7. Results from FE analysis and the correlation of results and features with each other. Data with label E (blue points) illustrate elastic behavior and data with label P (orange points) represent plastic behavior.

Table 7. Number of data based on the behavior of the system.

System behavior	Number of models in each category
Plastic	127
Elastic	38

- Only 23% of models remain in the elastic domain, see Table 7.

2. ML model

The current section details the development of a computational approach to predict the performance of a vast array of models. To achieve this goal, ML algorithms are utilized to train a machine, with the primary challenge being the optimization of hyper-parameters to improve machine performance. With sufficient accuracy, a trained machine can predict the performance of composite metal deck slabs under impact loading. Subsequent sections will illustrate the proper training of machines to predict the elastic and plastic behavior of these slabs. Initially, binary classification is employed to distinguish between elastic and plastic data, followed by regression to predict maximum negative moments and maximum deflection values based on key parameters.

2.1. Main steps of the ML model

This research utilizes an ML approach that involves three primary stages:

1. Importing, discovering, and visualizing the data to get insight;
2. Preparing the data for ML algorithms;
3. Selecting and training the models.

The initial phase involved importing the data as a CSV file into Google Colab. To organize the dataset, a data frame was examined. Additionally, the Seaborn library was utilized to create visual plots, as shown in Figure 7, providing a more comprehensive understanding of the raw data's initial condition. These tools distinctly illustrate that the dataset comprises 165 data points, and each data point is characterized by three primary features: slab length, striker weight, and striker velocity.

During the second phase, the dataset was prepared for the application of ML algorithms. The clarity of the data and the presence of missing values were assessed, and any issues were resolved. As some classification algorithms are sensitive to scaling, the data was standardized. The target values, plastic and elastic, were encoded to ensure that they were interpretable by the algorithms. Lastly, to evaluate the

accuracy and performance of the machines, the dataset was divided into training and testing sets.

The final step involved applying Scikit-Learn classification algorithms to prepare the data for binary classification, with the hyperparameters being fine-tuned. The following algorithms were used: K-Nearest Neighbors (KNN), Logistic Regression (LR), Decision Tree (DT), Random Forest (RF), Multilayer perceptron (MLP), Naive Bayes (NB), Stochastic Gradient Descent (SGD), and Support Vector Machine (SVM). In addition, Support Vector Regression (SVR) was utilized as the primary algorithm in the regression component.

2.2. Composite slabs behavior classification

In earlier sections, an assessment of the behavior of composite metal deck slabs was carried out via FE analysis. However, each analysis was found to be a time-consuming process, making it an impractical computational method for analyzing a large number of models. Consequently, to predict the elastic or plastic behavior of these slabs under impact loading, ML algorithms were employed. The trained machines are capable of making predictions on thousands of data points in under a minute, making them far more efficient and effective when compared to tedious FE analysis. The machines were trained for different algorithms, including KNN, LR, DT, RF, MLP, NB, SGD, and SVM, with their hyperparameters appropriately fine-tuned. Various algorithms were used during the training process to determine which performed better in classifying the dataset. The primary criteria for evaluating the performance of the trained machines were scores from cross-validation (with 3-fold) on the training set, the accuracy of predictions on test samples, F_1 score, and confusion matrix. The confusion matrix is a table that represents the performance of a trained machine in a classification problem and can be applied to a dataset where the actual label of data is specified. The values in the diagonal cells of the confusion matrix illustrate that the predicted labels by the machines for the data are true and equal to the actual labels.

In binary classification, the values are commonly referred to as True Negative (t_n) and True Positive (t_p), which are found in the diagonal cells of the confusion matrix. The non-diagonal cells contain values that indicate the difference between the predicted and actual labels, which are called False Positive (f_p) or False Negative (f_n) in binary classification. Table 8 displays a schematic layout of the confusion matrix for a binary classification problem. The F_1 score, which is one of the performance evaluation criteria for trained machines, can be computed using the precision and recall values from the confusion matrix, as demonstrated by Eqs. (3), (4), and (5):

Table 8. Schematic representation of confusion matrix in binary classification. Negative and positive are labels of data in this table.

Actual	**Predicted**	
	Negative	**Positive**
Negative	True negative	False positive
Positive	False negative	True positive

$$F_1 = \left(\frac{1}{recall^{-1}+precision^{-1}}\right) = 2 \times \frac{precision \times recall}{precision + recall}, \tag{3}$$

$$precision = \left(\frac{t_p}{t_p + f_p}\right), \tag{4}$$

$$recall = \left(\frac{t_p}{t_p + f_n}\right). \tag{5}$$

The machines that exhibited the best performance were trained using RF, SVM, and KNN algorithms, respectively. The hyperparameters optimized for these algorithms can be found in Table 9. The machine trained with the RF algorithm had zero errors and achieved exact predictions for both the training and test datasets. Conversely, the NB algorithm had the lowest accuracy with a score of only 91.7%. Table 10 outlines the precision, accuracy, and ranking of each algorithm used in the study. Additionally, Figure 8 presents a 3D plot of the predictions made by the top-ranked machine on the elastic region. The classification results for this dataset indicated that RF, SVM, and KNN algorithms outperformed other methods. This outcome was not surprising, particularly for SVM, as it is known to be one of the most reliable classification methods for many problems. However, a potential drawback of SVM and RF methods is their training speed when applied to large datasets. Nonetheless, the small dataset size used in this study mitigated this weakness.

Figure 8 depicts the machine's predicted elastic region (green volume) and demonstrates its ability to capture all data points exhibiting elastic behavior. However, data points related to plastic behavior fall outside of this region. Despite this, one must question the reliability of the machine's predictions in comparison to FE analysis and experimental measurements. The small dataset used in this study necessitates additional information to confidently rely on the ML approach's prediction results for composite slab design. This assertion is supported by the results presented in Table 11, where reducing the training data by 10% while increasing the test sample size by the same amount led to less reliable predictions.

Table 9. Tuned hyperparameters for the first three ranked machines in the classification of composite slabs behavior.

Method	Tuned hyperparameters
RF	$n_{\text{estimators}} = 100$, Max depth=4, Max features=2 $\min_{\text{samples leaf}} = 0.001$, $\min_{\text{samples split}} = 0.01$
KNN	Number of neighbors = 3
SVM	$\gamma = 0.1$ kernel=rbf $C = 100$

Table 10. Performance of trained machines in the classification of data with train set size equal to 0.85 dataset.

Method	Rank	Average CV score (%)	Test prediction accuracy (%)	Train data F_1 score (%)	Test data F_1 score (%)
RF	1	96.4	100.0	100.0	100.0
SVM	3	97.1	100.0	98.6	100.0
KNN	2	90.8	100.0	98.6	100.0
MLP	4	92.3	95.8	100.0	97.0
LR	5	93.6	100.0	96.4	100.0
SGD	6	91.5	100.0	95.5	100.0
DT	7	92.8	92.0	97.8	91.4
NB	8	87.2	91.7	89.5	94.1

Table 11. Performance of trained machines in the classification of data with train set size equal to 0.75 of the dataset.

Method	Rank	Average CV score (%)	Test prediction accuracy (%)	Train data F_1 score (%)	Test data F_1 score (%)
KNN	1	90.2	100.0	98.4	100.0
RF	2	95.1	95.2	100	96.8
SVM	3	95.9	95.2	98.9	96.8

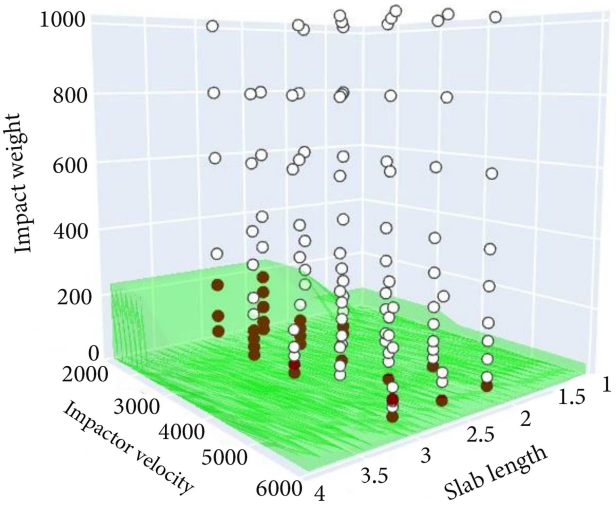

Figure 8. 3D illustration of prediction obtained by Random Forest algorithm. The white and red points represent the data with plastic and elastic labels in the training set respectively. The green volume shows the prediction of the machine for the elastic region.

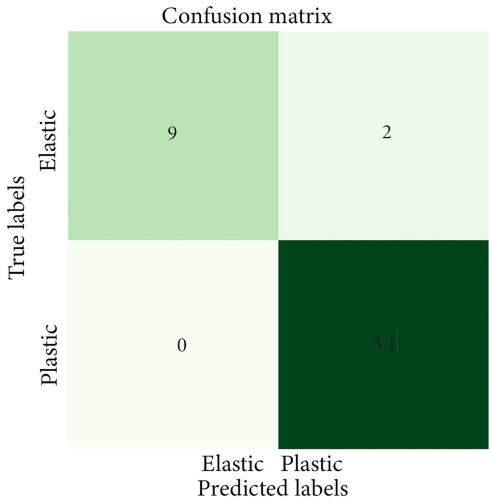

Figure 9. Confusion-matrix for test dataset when the machine is trained by Random Forest algorithm on a train dataset size equal to 0.75 of the whole dataset.

The performance of the machines is negatively affected by reducing the size of the training dataset, with errors primarily occurring in the prediction of data in the elastic region. The previous test set included seven data points labeled as elastic, whereas the new test set included 11 such points. The RF algorithm made all of its mistakes in only two of the new test set's elastic-labeled data points. This concentration of errors in a smaller portion of the data (as shown in the confusion matrix in Figure 9) can result in uncer-

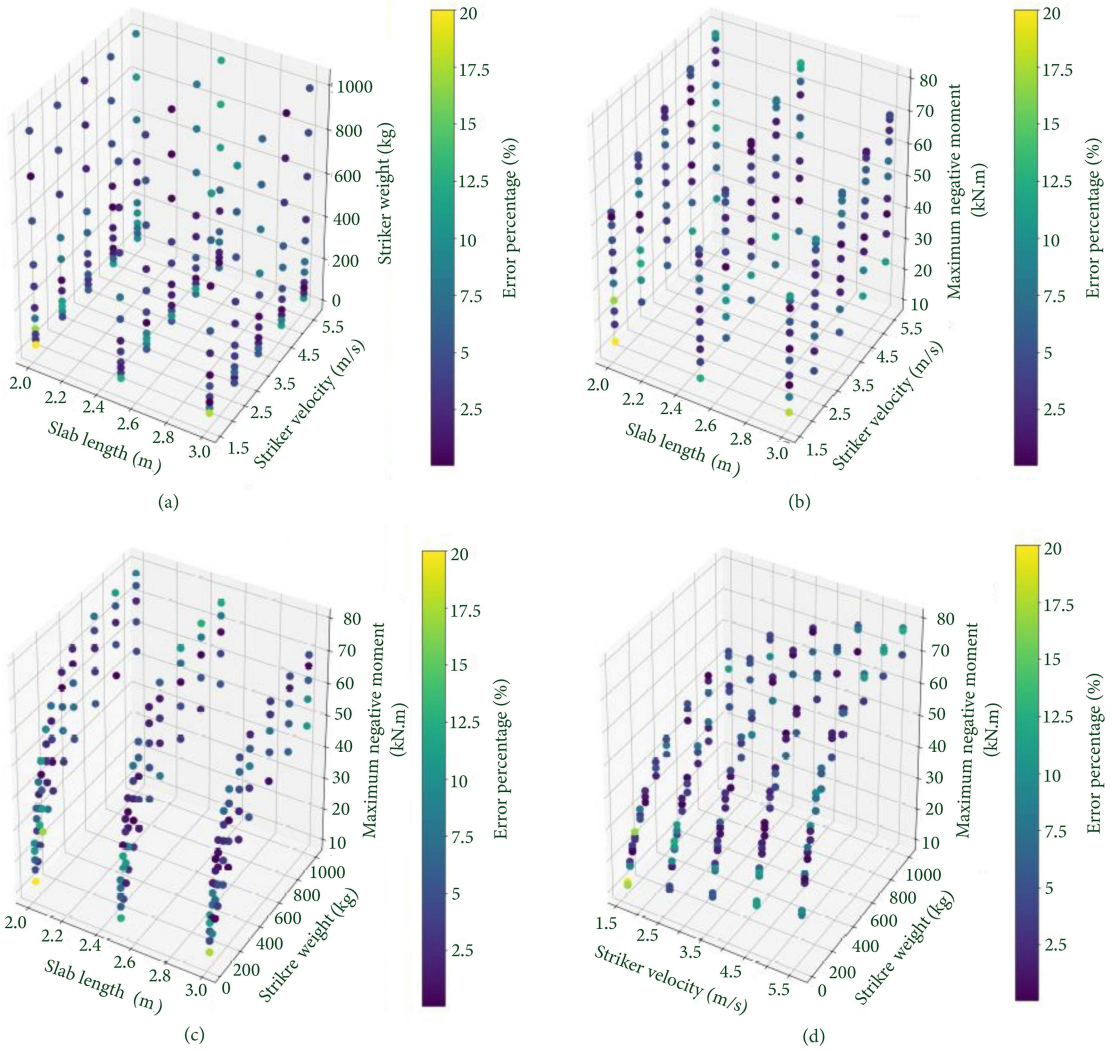

Figure 10. Prediction of the trained machine on maximum negative moments in composite metal deck slabs.

tainty regarding the machine's performance. However, these errors have a positive aspect as they lead to a more conservative design approach. If a specimen remains in the elastic domain, but the prediction is for plastic behavior, then the designers must improve the performance of the specimens by modifying the reinforcement or geometry, which results in overdesigning a component. Conversely, if the machine misidentifies a plastic specimen as elastic, it leads to design failure. Therefore, a larger test dataset can help produce more conservative design and prediction results. To enhance the reliability of the trained machines, more data with a more random distribution is needed, with particular emphasis on the border between the elastic and plastic regions.

2.3. Prediction of maximum negative moment and deflection

The design of composite metal deck slabs requires consideration of both deflection and negative moments.

Table 12. Tuned hyperparameters for machines doing regression for negative moments and deflections.

Regression target	Tuned hyper parameters
Moment	$\gamma = 0.2$, $C = 5$, $\varepsilon = 0.05$
Deflection	$\gamma = 0.05$, $C = 50$, $\varepsilon = 0.05$

To obtain data for these properties, previous studies used FE analysis and selected logarithmic scales for the parameters and target values. The machines were then trained on the scaled dataset, and their hyperparameters were optimized for performance. Table 12 presents the values of other hyperparameters such as C, γ, and ϵ. The results of the prediction based on the maximum negative moments are illustrated in Figure 10, with the color bars indicating the percentage difference between the predicted and actual values of the maximum negative moment at each point. Figure 10(a) shows the normal distribution of errors in estimating the maximum negative moments based on the three

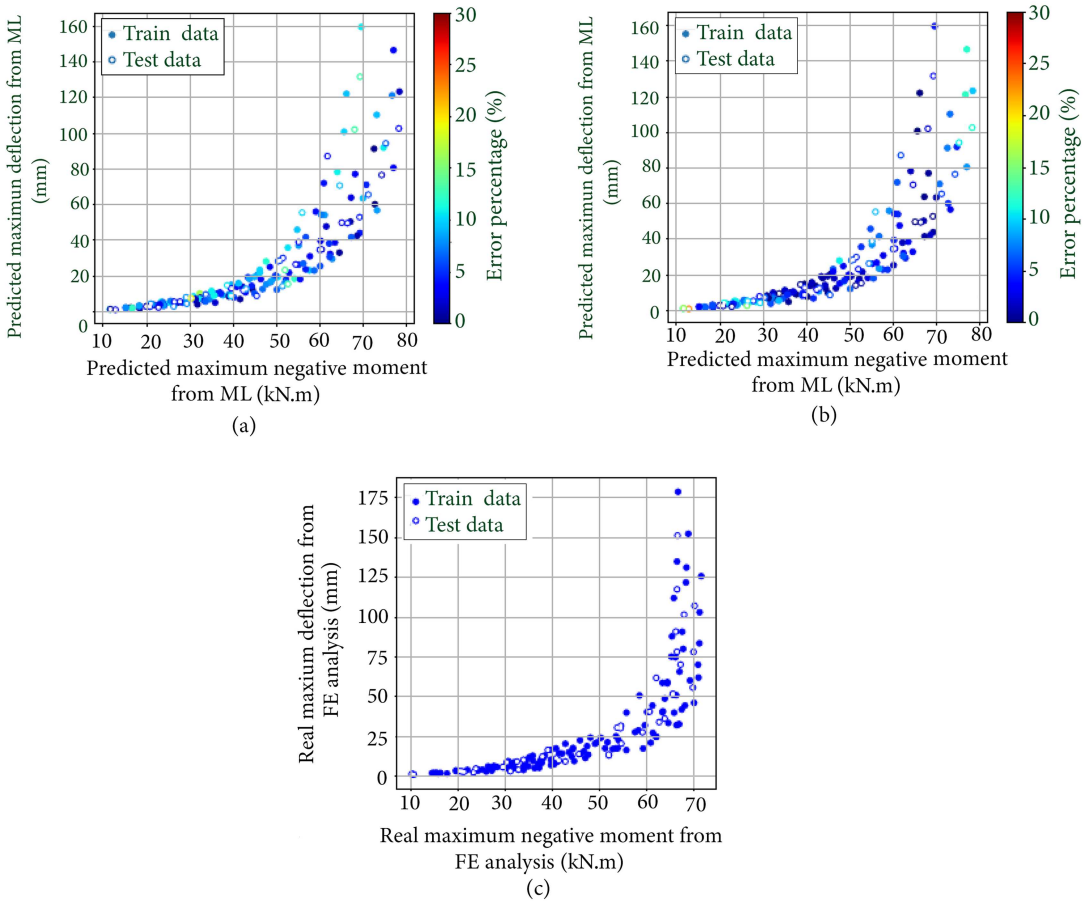

Figure 11. Maximum negative moment versus maximum deflection which is obtained from Finite Element (FE) analysis and machine learning approach: (a) Error percentage for deflections are illustrated in data point color; (b) Error percentage for negative moments are illustrated in data point color; and (c) Real data from FE analysis.

parameters, with no noticeable concentration of biased predictions in any particular region.

This indicates that the machine's predictions have been appropriately weighted for different regions, which is due to the proper preparation and scaling of data before algorithm application. Figure 10(d) illustrates the trend of maximum negative diagrams based on striker weight and velocity. Comparing the impact of these two parameters on the diagram slopes reveals the stronger influence of striker weight, which is also evident by examining Figure 10(c) and (b). In conclusion, the trained machines produce reasonable predictions of maximum negative moment values, with striker weight and velocity having a significant impact on the results.

The ML model for predicting maximum negative moments in composite slabs is trained using deflection target values, including hyper parameters tuning as shown in Table 12. The trained model can predict maximum deflections with a square root mean square error of 3.49 and 4.59 for train and test data, respectively. Figure 11 demonstrates the model's performance in predicting moment versus deflection diagrams. Figure 11(c) shows the actual dataset, while Figure 11(a) and (b) depict the model's predictions. The trained model captures the total trace in the moment-deflection diagram. Figure 11(a) color-codes the data points based on the percentage error in deflection prediction, with the highest error being around 19%. Similarly, Figure 11(b) color-codes the data points based on the percentage error in predicting maximum negative moments, with the maximum observed error being around 22%.

Upon comparing the images, it is evident that the difference between the predicted and actual deflections is more than 140 mm, making it impossible to express the difference in percentage. However, in the elastic domain, the difference between the predicted and actual deflections is comparatively small and can be expressed in terms of error percentages. The errors in both diagrams are distributed reasonably and the images containing error data can be relied upon to monitor the performance of the machine from the aspect of overfitting. The test and train data in the dataset are uniform and compatible, indicating that the machine is not solely reliant on the initial training

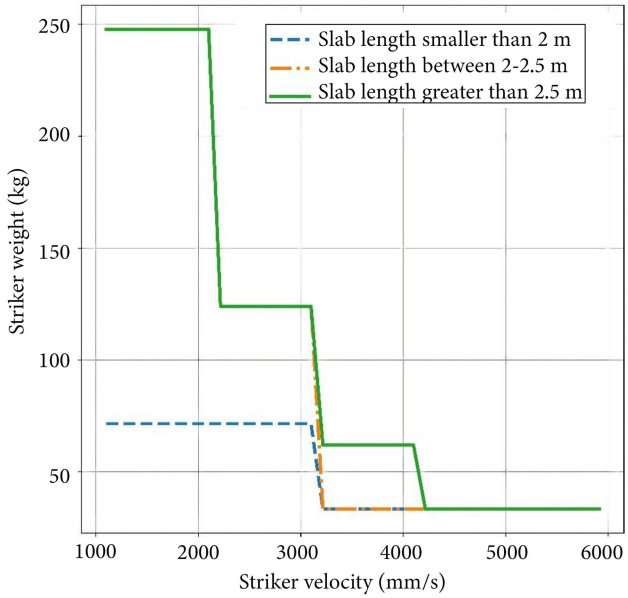

Figure 12. Sections from the elastic domain in constant values of slab length.

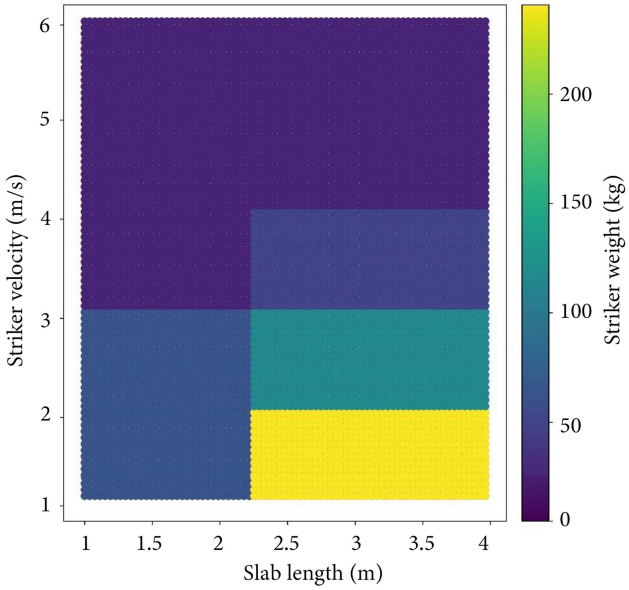

Figure 13. Sections from the elastic domain in constant values of striker weights.

data and can make accurate predictions on the test data as well.

3. Discussion

In the previous sections, the performance of composite metal deck slabs under free drop weight impact loading was examined using a ML approach and Finite Element (FE) analysis. The elastic domain of these slabs was determined based on the results obtained from the trained machines, as shown in Figure 8. For a better understanding of changes in the elastic domain, some sections were taken from the constant slab length and plotted, as shown in Figure 12. It was observed that the diagrams of striker weight against striker velocity for the three groups of slabs showed step charts, which are the primary features of the RF algorithm's predictions. Additionally, a visible elastic area was present under the diagrams when the striker velocity was below 3 m/s.

Increasing the length of the slab was found to increase the potential for the slabs to remain in the elastic domain. However, for short slabs with a length smaller than 2 m, the elastic capacity was observed to be reduced. The trend of the sections in Figure 12 confirmed that the elastic capacity in regions where the striker velocity exceeded 4 m/s was not significant. Figure 13 presents a different assessment of the striker velocity versus slab length in the elastic domain. The rectangular patterns in the figure indicate the use of the RF algorithm, while the color bar specifies the value of the striker weight in each step. The yellow region of the elastic domain corresponds to a high-weight striker with a velocity lower than 2 m/s and slab length greater than 2 m, whereas the purple region indicates a low-weight striker with a velocity greater than 4 m/s. Other regions denote the elastic domain based on the combination of features.

To gain a better understanding of the problem, the trained machines in the regression part can be utilized to obtain additional results. Figure 14 illustrates the performance of the trained machines in predicting data for slabs with a length of 2 m. Figure 14(a) compares the predictions of the machine for a maximum simulated negative moment and the actual moment values from the dataset versus striker weight. The machine performs well in predicting moments when the striker velocity is below 3.6 m/s. However, for higher striker velocity values, the predictions become less precise, particularly for heavier strikers. The errors in the high-velocity domain become more significant with heavier strikers. Figure 14(b) shows the maximum deflection predicted by the machine versus striker weight. It is apparent that the errors in predictions are uniformly distributed along the diagram trace. To evaluate the performance of the trained machines, the formulas proposed by Emami and Kabir [25] can be employed. The proposed formulas, namely Eqs. (6) and (7), are calibrated as follows:

$$u = 0.0684 \times m + 7.3685, \tag{6}$$

$$M = \begin{cases} -0.0272 \times (24.8 \times ln(0.0684m + 7.3685) + 292.89)^2 \\ \quad +17.93 \times (24.8 \times ln(0.0684m + 7.3685) + 292.89) \\ \quad -2988.8 \qquad 50 \leq m \leq 200 \\ \\ -0.0272 \times (24.8 \times ln(0.0684m + 7.3685) + 292.89)^2 \\ \quad +17.93 \times (3.7508 \times ln(0.0684m + 7.3685) + 355.31) \\ \quad -2988.8 \qquad 200 \leq m \leq 2200 \end{cases} \tag{7}$$

These formulas use to represent deflection and to indicate the maximum negative moment, while m

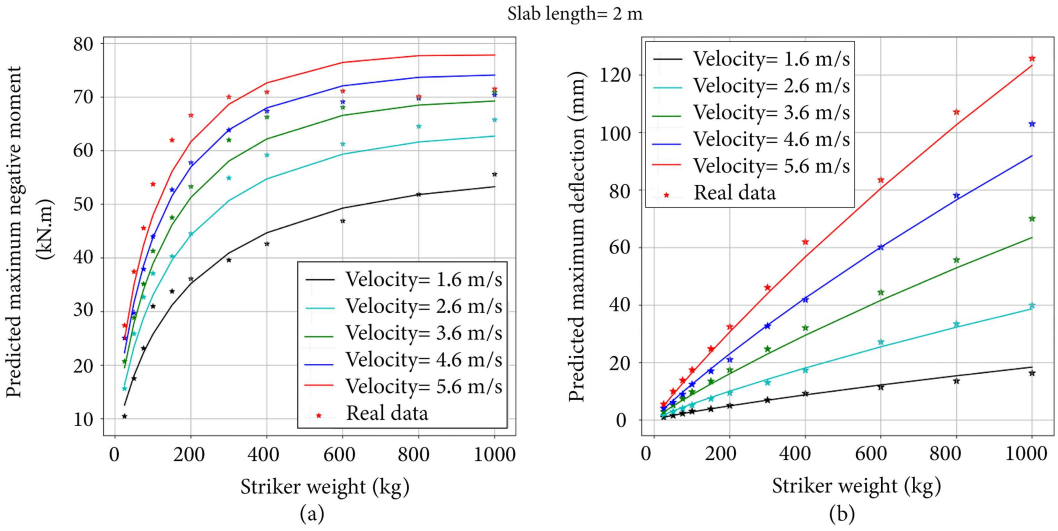

Figure 14. Machine's performance in prediction of the maximum negative moment and maximum deflection in slabs with 2 m in length.

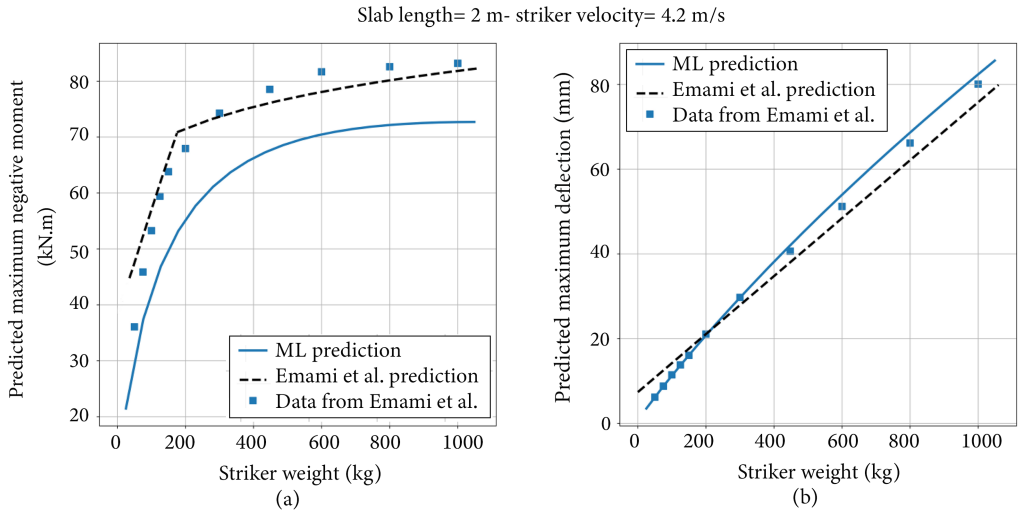

Figure 15. Comparison between the trained machine's predictions and the formula which were proposed by Emami and Kabir [25].

represents the weight of the striker. Figure 15(a) and (b) compare the results obtained from the prediction of the trained machines and the results from the proposed formulas. It is observed that there is a discrepancy of about 15% in predicting the ultimate negative moment of the systems. This difference can be explained in a few ways. Firstly, both methods are predictive, so there may be some variation in the results. Secondly, there is significant inconsistency at the beginning of the diagrams with lighter strikers, whereas the suggested formula is suitable for strikers heavier than 50 kg. Additionally, the dissimilarity between these two predictions seems to be linked to the method of applying contact type between the metal deck and rigid fixture in the FE model. As explained earlier, Emami and Kabir [25] assumed the contact between the rigid fixture and metal deck to be a fully tied contact. However, in the present study, only the elements around the shear studs, which are similar to welded regions in real slabs, were assumed to be tied to the rigid fixture, and other regions had normal friction contact. This may decrease the maximum negative moment carrying capacity of the sections near the support region.

The ML predictions for maximum deflections are closer to previous measurements compared to ultimate negative moments, as shown in Figure 15(b). The change in contact type between the metal deck and rigid fixture also affects the predictions, particularly for high deflection values. The trained machines can be used to extend the results, as seen in Figures 16–19, which show predictions for maximum negative

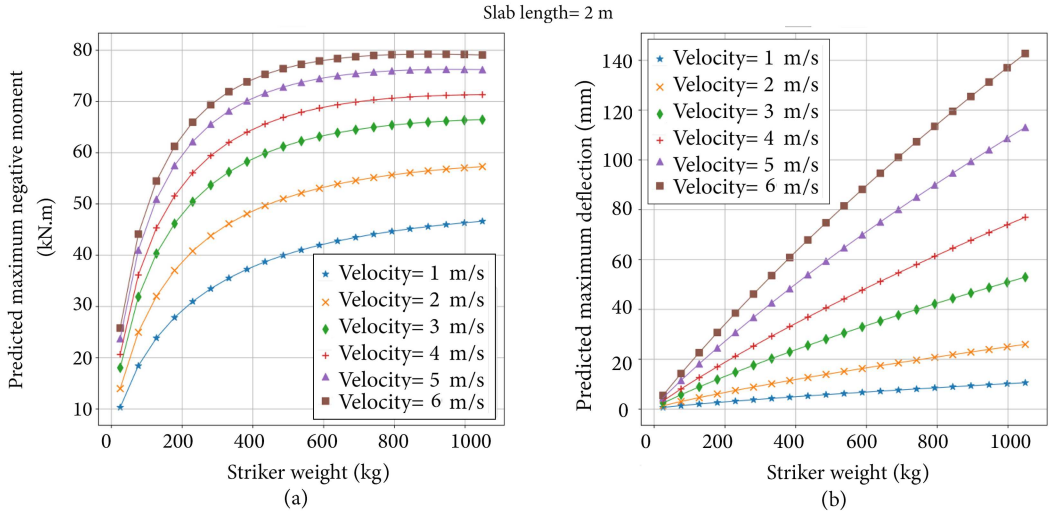

Figure 16. Machine's performance in prediction of the maximum negative moment and maximum deflection in slabs with 2 m in length.

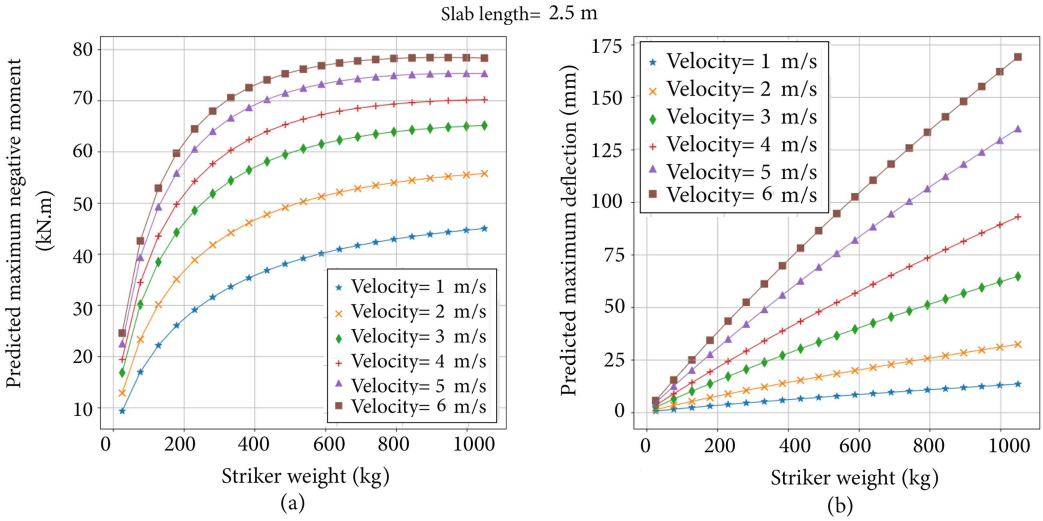

Figure 17. Machine's performance in prediction of the maximum negative moment and maximum deflection in slabs with 2.5 m in length.

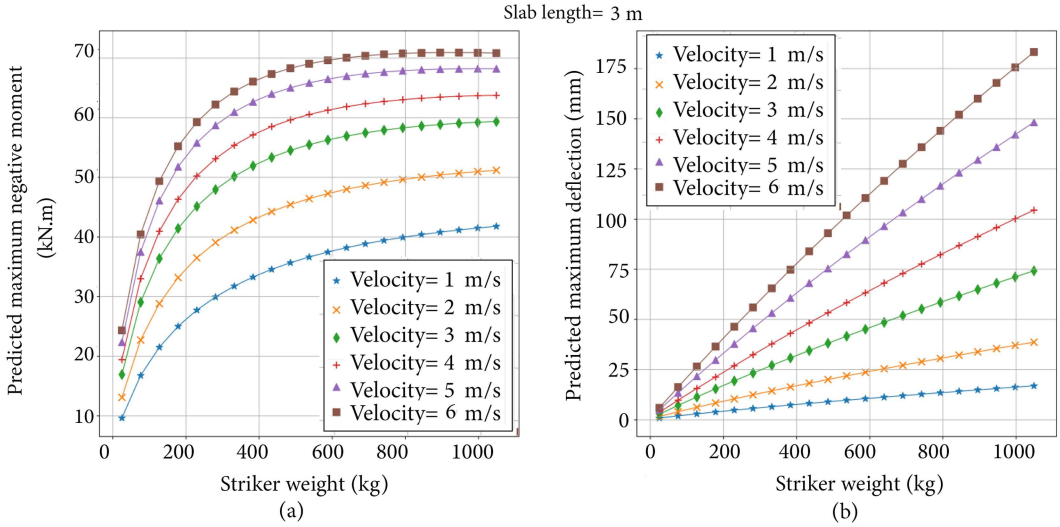

Figure 18. Machine's performance in prediction of the maximum negative moment and maximum deflection in slabs with 3 m in length.

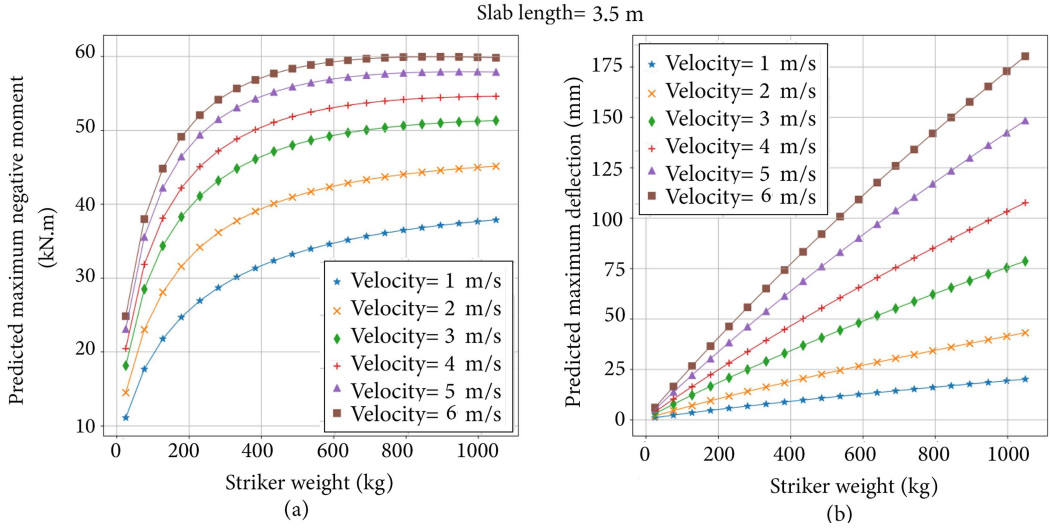

Figure 19. Machine's performance in prediction of the maximum negative moment and maximum deflection in slabs with 3.5 m in length.

moments and maximum deflections of composite metal deck slabs in common lengths of 1–4 meters. The nonlinear trend for maximum negative moments and linear trend for maximum deflections are notable features. For a constant slab length and striker velocity, the systems gradually reach their moment bearing capacity as striker weight increases. This trend is more pronounced with higher striker velocity. When velocities exceed 1 m/s, the maximum negative moment diagrams become flat lines once striker weight approaches 1000 kg, indicating the slabs have reached their ultimate moment capacity for such weights. Further increases in striker weight beyond these limits may cause more damage in the material's plastic state. The maximum negative moments achievable by these slabs range from 60 to 80 kN.m, but this range is only applicable when the striker velocities and weights do not exceed 1 m/s and 1000 kg, respectively.

4. Conclusions

This study investigates the behavior of composite metal deck slabs subjected to impact loading using two computational tools: Finite Element (FE) analysis and Machine Learning (ML). A total of 165 FE models were generated to explore the effect of slab length, striker velocity, and striker weight on the maximum negative moments and deflections. The results show that the striker velocity and weight have a considerable impact on the behavior of composite slabs under impact loading.

To enhance the computational method's efficiency in terms of cost and time, a machine-learning approach was employed after the FE analysis. The main objective of this approach was to train machines with high accuracy to predict the performance of numerous models in a short duration. The dataset used for training the machines consisted of the initial data and outcomes of the parametric study. The desired tasks for the machines were to make predictions on the slabs' elastic and plastic behavior, as well as the maximum negative moment and maximum deflection.

After the machines were trained and the hyper parameters were tuned, the Random Forest (RF), K-Nearest Nighbor (KNN), and Support Vector Machine (SVM) algorithms demonstrated the most effective performance in classifying the elastic and plastic behavior of composite slabs under impact loading. Because the dataset was small and straightforward, and the features were correlated with each other in order, the machine trained with the RF algorithm was able to predict with 100% F_1 and test scores. In this machine, the average cross-validation score within three folds was over 96% consistent. Using the trained machine, elastic and plastic behavior domains of these slabs were determined, and the characteristics of these domains were analyzed. It was discovered that slabs longer than 2.5 m can provide higher elastic capacity. The significant influence of striker velocity and weight on the plastic behavior of these slabs was also taken into consideration.

The machines were trained using the SVR algorithm for predicting the maximum negative moments and maximum deflections. After hyperparameter tuning, the trained machines were able to produce accurate predictions with low error. The machines captured the overall trend in the negative moment versus deflection diagrams and were able to predict the negative moment amounts in both the plastic and elastic domains. The influence of each feature on the prediction results was discussed, and the accuracy of the results was compared to FE results and current

data. It was observed that at high striker velocities, the specimens exhibited an ultimate internal negative moment ranging from 60 to 80 kN.m.

List of notations

ε_{ult}	Steel ultimate strain
$DIF_{steel\ yield}$	Dynamic increase factor for steel yield stress
$DIF_{steel\ failure}$	Dynamic increase factor for steel ultimate stress
$\dot{\varepsilon}$	Steel strain rate
f_y	Steel yield stress
f_u	Steel ultimate stress
F_1	Score for evaluating trained machines performance
u	Maximum deflection
m	Weight of striker
M^-	Maximum negative moment

References

1. Evans, H.R. and Wright, H.D. "Steel-concrete composite flooring deck structures", *CRC Press*, pp. 31–62 (1988). https://www.taylorfrancis.com/chapters/edit/10.1201/9781482286366-4/steel
2. Mohammed, B.S., Al-Ganad, M.A., and Abdullahi, M. "Analytical and experimental studies on composite slabs utilising palm oil clinker concrete", *Constr Build Mater*, **25**, pp. 3550–3560 (2011). https://doi.org/10.1016/J.CONBUILDMAT.2011.03.048
3. Ma, W., Becque, J., Hajirasouliha, I., et al. "Cross-sectional optimization of cold-formed steel channels to Eurocode 3", *Eng Struct.*, **101**, pp. 641–651 (2015). https://doi.org/10.1016/j.engstruct.2015.07.051
4. Lowe, D., Roy, K., Das, R., et al. "Full scale experiments on splitting behaviour of concrete slabs in steel concrete composite beams with shear stud connection", *Structures*, **23**, pp. 126–138 (2020). https://doi.org/10.1016/j.istruc.2019.10.008
5. Ye, J., Hajirasouliha, I., Becque, J., et al. "Optimum design of cold-formed steel beams using Particle Swarm Optimisation method", *J Constr Steel Res.*, **122**, pp. 80–93 (2016). https://doi.org/10.1016/j.jcsr.2016.02.014
6. Hedaoo, N.A., Gupta, L.M., and Ronghe, G.N. "Design of composite slabs with profiled steel decking: a comparison between experimental and analytical studies", *International Journal of Advanced Structural Engineering*, **4**, pp. 1–15 (2012). https://doi.org/10.1186/2008-6695-3-1
7. Fang, Z., Fang, H., Huang, J., et al. "Static behavior of grouped stud shear connectors in steel-precast UHPC composite structures containing thin full-depth slabs", *Eng Struct.*, **252**, 113484 (2022). https://doi.org/10.1016/j.engstruct.2021.113484
8. Zineddin, M. "Dynamic response and behavior of reinforced concrete slabs under impact loading", *Int J Impact Eng.*, **34**, pp. 1517–1534 (2007). https://doi.org/10.1016/J.IJIMPENG.2006.10.012
9. Wang, W., Zhang, D., Lu, F., et al. "Experimental study and numerical simulation of the damage mode of a square reinforced concrete slab under close-in explosion", *Eng Fail Anal.*, **27**, pp. 41–51 (2013). https://doi.org/10.1016/J.ENGFAILANAL.2012.07.010
10. Yao, S., Zhang, D., Chen, X., et al. "Experimental and numerical study on the dynamic response of RC slabs under blast loading", *Eng Fail Anal.*, **66**, pp. 120–129 (2016). https://doi.org/10.1016/J. ENGFAILANAL.2016.04.027
11. Thiagarajan, G., Kadambi, A.V., Robert, S., et al. "Experimental and finite element analysis of doubly reinforced concrete slabs subjected to blast loads", *Int J Impact Eng.*, **75**, pp. 162–173 (2015). https://doi.org/10.1016/J.IJIMPENG.2014.07.018
12. Yankelevsky, D.Z., Karinski, Y.S., and Feldgun, V.R. "Dynamic punching shear failure of a RC flat slab-column connection under a collapsing slab impact", *Int J Impact Eng.*, **135**, pp. 103401 (2020). https://doi.org/10.1016/J.IJIMPENG.2019.103401
13. Sainz-Aja, J., Pombo, J., Tholken, D., et al. "Dynamic calibration of slab track models for railway applications using full-scale testing", *Comput Struct.*, **228**, p. 106180 (2020). https://doi.org/10.1016/J.COMPSTRUC.2019.106180
14. Yang, B., Wang, H., Yang, Y., et al. "Numerical study of rigid steel beam-column joints under impact loading", *J Constr Steel Res*, **147**, pp. 62–73 (2018). https://doi.org/10.1016/j.jcsr.2018.04.004
15. Zhao, L., Yu, Z.X., Liu, Y.P., et al. "Numerical simulation of responses of flexible rockfall barriers under impact loading at different positions", *J Constr Steel Res*, **167**, 105953 (2020). https://doi.org/10.1016/j.jcsr.2020.105953
16. Huo, J., Wang, H., Li, L., et al. "Experimental study on impact behaviour of stud shear connectors in composite beams with profiled steel sheeting", *J Constr Steel Res*, **161**, pp. 436–449 (2019). https://doi.org/10.1016/j.jcsr.2018.04.029
17. Guo, Q. and Zhao, W. "Design of steel-concrete composite walls subjected to low-velocity impact", *J Constr Steel Res*, **154**, pp. 190–196 (2019). https://doi.org/10.1016/j.jcsr.2018.12.001
18. Jung, J.-W., Yoon, Y.-C., Jang, H.W., et al. "Investigation on the resistance of steel-plate concrete walls under high-velocity impact", *J Constr Steel Res.*, **162**, 105732 (2019). https://doi.org/10.1016/j.jcsr.2019.105732

19. Sadraie, H., Khaloo, A., and Soltani, H. "Dynamic performance of concrete slabs reinforced with steel and GFRP bars under impact loading", *Eng Struct.*, **191**, pp. 62–81 (2019). https://doi.org/10.1016/J.ENGSTRUCT.2019.04.038

20. Zhao, C., Lu, X., Wang, Q., et al. "Experimental and numerical investigation of steel-concrete (SC) slabs under contact blast loading", *Eng Struct.*, **196**, 109337 (2019). https://doi.org/10.1016/J.ENGSTRUCT.2019.109337

21. Al Rawi, Y., Temsah, Y., Baalbaki, O., et al. "Experimental investigation on the effect of impact loading on behavior of post- tensioned concrete slabs", *Journal of Building Engineering*, **31**, 101207 (2020). https://doi.org/10.1016/J.JOBE.2020.101207

22. Guo, J., Cai, J., and Chen, W. "Inertial Effect on RC Beam Subjected to Impact Loads", *International Journal of Structural Stability and Dynamics*, **17**, 1750053 (2016). https://doi.org/10.1142/S0219455417500535

23. Kong, X., Fang, Q., Wu, H., et al. "Numerical predictions of cratering and scabbing in concrete slabs subjected to projectile impact using a modified version of HJC material model", *Int J Impact Eng.*, **95**, pp. 61–71 (2016). https://doi.org/10.1016/J.IJIMPENG.2016.04.014

24. Izatt, C., May, I.M., Lyle, J., et al. "Perforation owing to impacts on reinforced concrete slabs", *Proceedings of the Institution of Civil Engineers-Structures and Buildings*, **162**, pp. 37–44 (2009). https://doi.org/10.1680/stbu.2009.162.1.37

25. Emami, F. and Kabir, M.Z. "Performance of composite metal deck slabs under impact loading", *Structures*, **19**, pp. 476–489 (2019). https://doi.org/10.1016/j.istruc.2019.02.015

26. Ding, X., Hasanipanah, M., Nikafshan Rad, H., et al. "Predicting the blast-induced vibration velocity using a bagged support vector regression optimized with firefly algorithm", *Eng Comput.*, **37**, pp. 2273–2284 (2021). https://doi.org/10.1007/s00366-020-00937-9

27. Kabir, H. and Garg, N. "Machine learning enabled orthogonal camera goniometry for accurate and robust contact angle measurements", *Scientific Reports*, **13**(1), 1497 (2023). https://doi.org/10.1038/s41598-023-28763-1

28. Kardan, Y.H.J.-B.-O. and authorMohammad-T.A. "Experimental and numerical investigation of bridge pier scour estimation using ANFIS and teaching–learning-based optimization methods", *Eng Comput.*, **35**, pp. 1103–1120 (2019).

29. Naser, M.Z. "Can past failures help identify vulnerable bridges to extreme events? A biomimetical machine learning approach", *Eng Comput.*, **37**(2), pp. 1099–1131 (2021).

30. Kiani, J., Camp, C., and Pezeshk, S. "On the application of machine learning techniques to derive seismic fragility curves", *Comput Struct.*, **218**, pp. 108–122 (2019). https://doi.org/10.1016/J.COMPSTRUC.2019.03.004

31. Zhang, R., Chen, Z., Chen, S., et al. "Deep long short-term memory networks for nonlinear structural seismic response prediction", *Comput Struct.*, **220**, pp. 55–68 (2019). https://doi.org/10.1016/J.COMPSTRUC.2019.05.006

32. Sakong, J., Woo, S.-C., and Kim, T.-W. "Determination of impact fragments from particle analysis via smoothed particle hydrodynamics and k-means clustering", *Int J Impact Eng.*, **134**, 103387 (2019). https://doi.org/10.1016/J.IJIMPENG.2019.103387

33. Bortolan Neto, L., Saleh, M., Pickerd, V., et al. "Rapid mechanical evaluation of quadrangular steel plates subjected to localised blast loadings", *Int J Impact Eng.*, **137**, 103461 (2020). https://doi.org/10.1016/J.IJIMPENG.2019.103461

34. Capuano, G. and Rimoli, J.J. "Smart finite elements: A novel machine learning application", *Comput Methods Appl Mech Eng.*, **345**, pp. 363–381 (2019). https://doi.org/10.1016/J.CMA.2018.10.046

35. Feng, Y., Gao, W., Wu, D., et al. "Machine learning aided stochastic elastoplastic analysis", *Comput Methods Appl Mech Eng.*, **357**, 112576 (2019). https://doi.org/10.1016/J.CMA.2019.112576

36. Zohdi, T.I. "Dynamic thermomechanical modeling and simulation of the design of rapid free-form 3D printing processes with evolutionary machine learning", *Comput Methods Appl Mech Eng.*, **331**, pp. 343–362 (2018). https://doi.org/10.1016/J.CMA.2017.11.030

37. Wu, J.-L., Sun, R., Laizet, S., et al. "Representation of stress tensor perturbations with application in machine-learning-assisted turbulence modeling", *Comput Methods Appl Mech Eng.*, **346**, pp. 707–726 (2019). https://doi.org/10.1016/J.CMA.2018.09.010

38. Fang, Z., Roy, K., Mares, J., et al. "Deep learning-based axial capacity prediction for cold-formed steel channel sections using Deep Belief Network", *Structures.*, **33**, pp. 2792–2802 (2021). https://doi.org/10.1016/j.istruc.2021.05.096

39. Fang, Z., Roy, K., Chen, B., et al. "Deep learning-based procedure for structural design of cold-formed steel channel sections with edge-stiffened and un-stiffened holes under axial compression", *Thin-Walled Structures.*, **166**, 108076 (2021). https://doi.org/10.1016/j.tws. 2021.108076

40. Fang, Z., Roy, K., Mares, J., et al. "Deep learning-based axial capacity prediction for cold-formed steel channel sections using Deep Belief Network", *Structures*, **33**, pp. 2792–2802 (2021). https://doi.org/10.1016/j.istruc.2021.05.096

41. Fang, Z., Roy, K., Ma, Q., et al. "Application of deep learning method in web crippling strength prediction of cold-formed stainless steel channel sections under

end-two-flange loading", *Structures*, **33**, pp. 2903–2942 (2021). https://doi.org/10.1016/ j.istruc.2021.05.097

42. Bligh, Y.D.M.A.A.-O. and R. "Evaluation of LS-DYNA Concrete Material Model 159", *United States, Federal Highway Administration, Office of Research* (2007).
43. Castedo, R., Segarra, P., Alañon, A., et al. "Air blast resistance of full-scale slabs with different compositions: Numerical modeling and field validation", *Int J Impact Eng.*, **86**, pp. 145–156 (2015). https://doi.org/10.1016/J.IJIMPENG.2015.08.004
44. Sadiq, M., Xiu Yun, Z., and Rong, P. "Simulation analysis of impact tests of steel plate reinforced concrete and reinforced concrete slabs against aircraft impact and its validation with experimental results", *Nuclear Engineering and Design.* **273**, pp. 653–667 (2014). https://doi.org/10.1016/J.NUCENGDES.2014.03.031
45. Saini, D. and Shafei, B. "Concrete constitutive models for low velocity impact simulations", *Int J Impact Eng.*, **132**, 103329 (2019). https://doi.org/10.1016/J.IJIMPENG.2019.103329
46. Alañón, A., Cerro-Prada, E., Vázquez-Gallo, M.-J., et al. "Mesh size effect on finite-element modeling of blast-loaded reinforced concrete slab", *Eng Comput.* **34**, pp. 649–658 (2018).
47. Murray, Y.D. "Users Manual for LS-DYNA Concrete Material Model 159", *United States, Federal Highway Administration, Office of Research* (2007).
48. ASTM: ASTM C136/C136M-14 "Standard Test Method for Sieve Analysis of Fine and Coarse Aggregates", *ASTM International*, West Conshohocken. (2014). https://doi.org/10.1520/ C0136-C0136M-14
49. ASTM: A370 "Standard Test Methods and Definitions for Mechanical Testing of Steel Products", (2014).
50. "CEB-FIP model code 1990: design code", London: Telford (1993).

Biographies

Fakhreddin Emami a PhD student at the University of South Carolina, has a strong interest in the computational mechanics of metamaterials. He utilizes a diverse range of computational tools to create novel materials that possess extraordinary properties that are not naturally occurring.

Mohammad Zaman Kabir is a Professor of Structures and Solid Mechanics at the Department of Civil and Environmental Engineering at Amir Kabir University of Technology in Tehran, Iran. Professor Kabir earned his PhD in 1995 from the Solid Mechanics Division at the Department of Civil Engineering at the University of Waterloo in Ontario, Canada, where his research focused on the stability of thin-walled laminated composite members. Professor Kabir has authored numerous papers on topics such as composite structures, structural stability, structural optimization, prefabricated sandwich panels, and retrofitting structures using FRP fabrics. His current research interests include strengthening structures under excessive loading, innovative materials for structures, lightweight structures, and the application of 3D printing in the civil engineering industry.